Heterostructured Au-Ir Catalysts for Enhanced Oxygen Evolution Reaction

Peng-Cheng Chen,[†,§] Mufan Li,[‖] Jianbo Jin,[§] Sunmoon Yu,[‖,#] Shouping Chen,[‖,#] Chubai Chen,[§] Miquel Salmeron,[#,⊥] and Peidong Yang[*,†,§,‖,#,⊥]

† Kavli Energy Nanoscience Institute, University of California, Berkeley, California 94720, United States

§ Department of Chemistry, University of California, Berkeley, California 94720, United States

‖ Chemical Sciences Division, Lawrence Berkeley National Laboratory, Berkeley, California 94720, United States

Department of Materials Science and Engineering, University of California, Berkeley, California 94720, United States

⊥ Materials Sciences Division, Lawrence Berkeley National Laboratory, Berkeley, California 94720, United States

*Corresponding Author: Peidong Yang, *email address*: p_yang@berkeley.edu

ABSTRACT

Electrochemical water splitting operated in acidic conditions provides a clean approach to generate hydrogen fuels. Currently, the sluggish kinetics of oxygen evolution reaction (OER) at the anode is a bottleneck limiting the acidic water splitting. Here, we report that the OER activity of Ir, one of the most commonly used OER catalysts, can be boosted by forming phase boundaries with Au. Mixed Au and Ir catalysts were synthesized on carbon paper electrodes, which underwent structural evolution under the OER environment to form an Au-Ir interface-rich structure. Compared with Ir catalyst, which requires an overpotential of ~393 mV to achieve a current density of 10 mA/cm^2 in 0.1 M $HClO_4$ electrolyte, the evolved Au-Ir catalyst shows a lower overpotential at ~351 mV. XPS study in conjunction with electrochemical analysis on the surface-site-normalized activity reveal that the improved OER performance is owing to the presence of Au-Ir interfaces in the catalysts. In addition to Ir, the strategy of accelerating OER via Au-Ir interfaces has been further applied to IrCo, IrNi, and IrCu alloy catalysts. With the broad applicability of the strategy demonstrated, this study opens a new route to design OER catalysts for efficient acidic water splitting.

MAIN TEXT

Electrochemical water splitting powered by renewable energy provides a clean and sustainable pathway to generate hydrogen, a promising energy carrier with high energy density and low environmental pollution.[1-8] Practically, water splitting can be conducted in acidic conditions using proton-exchange membrane water electrolyzers, which has many advantages including high current density, low gas crossover, and wide range of operational power.[1,2] However, the sluggish four-electron transfer process of oxygen evolution reaction (OER) at the anode limits the application of acidic water splitting.[4,6,9,10] Consequently, there is an urgent need to develop efficient catalysts that can boost OER to improve the overall efficiency of water splitting. From a fundamental perspective, the OER process in acidic environment is considered to include four elementary steps, wherein the H_2O is oxidized to form O_2 via the intermediates including *OH, *O, and *OOH.[4,9-12] OER catalysts generally exhibit linearly-related binding strength to these O-species despite the fact that an ideal catalyst should have strong binding to *OH in order to efficiently dissociate the water molecule while possesses a relatively weak binding to *O and *OOH such that the intermediates can be easily oxidized to form O_2.[4-6,11-14] This phenomenon is known as the scaling relation limit of catalysts.[13,15,16] To date, Ir is one of the most intrinsically active OER catalysts in acidic media. Ir possesses a strong binding to O-species, making it effective in dissociating H_2O but not in forming O_2.[11,14] In this regard, advances in improving the OER activity of Ir have been achieved by alloying Ir with other metals,[17-27] as well as tailoring the geometric morphology of Ir catalysts.[28-34] The underlying mechanism is to: (i) optimize the intrinsic electronic structure of Ir sites to reach the summit of the activity volcano plot, which is characteristic of catalysts restricted by the scaling relation; and (ii) increase the number of exposed Ir sites in the catalysts.

One alternative way to circumvent the scaling relation limit of catalysts is to incorporate different catalytic sites into one catalyst such that each site is responsible for a different step in the whole reaction process.[15,16] Importantly, by decoupling the reactant-activation and product-formation steps, one can accomplish a reaction that involves multiple steps in a tandem manner, thus bypassing the scaling relation limit of catalysts with a single type of catalytic sites. For example, AuNi nanoparticles have been reported to be a superior catalyst for CO_2 hydrogenation, where the surface Ni atoms are active for hydrogenating CO_2 to *CO, and the surface Au atoms facilitate the desorption of *CO and contribute to the high selectivity of CO.[35] In addition,

transition metal catalysts such as Co and Fe have been combined with lithium hydride to achieve an enhanced activity for ammonia synthesis.[36] The transition metal catalysts provide active sites for dissociating nitrogen (N_2) into *N while the *N intermediates can spillover to the lithium hydride and are subsequently reduced to form ammonia. Besides thermal catalysis,[35-38] the concept of tandem catalysis has also been employed in electrocatalysis.[39,40] For instance, Pt-$Ni(OH)_2$ hybrid catalysts were used for hydrogen evolution reaction in alkaline conditions.[39] It is believed that the $Ni(OH)_2$ can boost the dissociation of water molecules in alkaline electrolyte while the Pt adsorbs the *H intermediates and recombine them into H_2.

Inspired by the success of tandem catalysis in these reactions, we hypothesize that the OER activity of Ir can be improved by equipping it with a catalyst possessing weaker oxygen affinity to achieve tandem catalysis on OER. To this end, we chose Au as the second component of the hybrid catalysts due to its weaker binding ability towards O-species,[11,14] which may facilitate the oxidation of the intermediates to form O_2. Besides, Au and Ir are highly immiscible spanning a broad compositional and temperature range,[41] which will ensure a phase-separated structure between these two metals. To date, there have been a few reports on using AuIr bimetallic catalysts for enhanced OER.[20,21,31-34] However, the activity improvement is generally attributed to the increased intrinsic activity of Ir sites because of the electron transfer either from Au to Ir[20] or from Ir to Au.[21,33] It remains unclear whether Au and Ir can be integrated as a phase-separated catalyst to perform OER tandem catalysis across the Au-Ir interfaces. To validate this hypothesis, we prepared mixed Au and Ir catalysts on carbon paper electrodes by drop-cast and thermal decomposition of their salt precursors. Notably, we observed the structural evolution of the mixed Au and Ir catalysts when the catalysts were used for electrochemical OER, which resulted in Au-Ir particles with larger sizes and enriched in Au-Ir phase boundaries. The heterostructured Au-Ir catalysts exhibit enhanced OER activity as compared to the monometallic counterparts. Furthermore, we found that the OER activity of Ir-based alloy catalysts, such as IrCo, IrNi, and IrCu, can also be boosted by forming heterostructures with Au.

The Au-Ir catalysts were synthesized by drop-casting equivalent amount of gold(III) chloride and Iridium(IV) chloride onto carbon paper supports and then thermally annealing the carbon papers under flowing Ar/H_2 (Fig. 1A). High-angle annular dark-field scanning transmission electron microscopy (HAADF-STEM), energy dispersive X-ray spectroscopy (EDS), and high-resolution transmission electron microscopy (HRTEM) characterizations were carried out on the

catalysts to investigate the composition and structure of the catalysts. As can be seen in Figure 1B-1D, S1, and S2, the catalysts are composed of Au and Ir particles with a broad size distribution (Au: 10-40 nm; Ir: 2-15 nm) and uneven dispersion on the carbon paper supports. In addition, both heterostructured Au-Ir particles and separated monometallic particles are present in the catalysts. The low uniformity of the catalysts can be attributed to the uncontrolled nucleation, growth, and coarsening of the particles during the thermal synthesis process. When the catalysts were used for OER, the Au and Ir particles were found to agglomerate and transform into larger-size particles (10-250 nm, Fig. 1E, 1F and S3-S6). EDS elemental mapping of the catalysts after OER tests indicates that the evolved catalysts consist of both Au and Ir with an interface-rich structure (Fig. 1G and S2).

To further understand the structures of the Au-Ir catalysts, X-ray diffraction (XRD) was carried out on catalysts before and after OER tests (Fig. 2A). Compared with the carbon paper support (Fig. 2A, black line), XRD pattern of the catalyst before OER test exhibits two sets of new peaks that can be assigned to face-centered cubic (fcc) Au and fcc Ir crystal structures, respectively (Fig. 2A, blue line). The result is consistent with the EDS mapping result, where Au and Ir are clearly phase-separated. Notably, XRD pattern of the evolved catalyst also shows the peaks at the same diffraction angles, indicating that Au and Ir remain a phase-separated state after OER tests (Fig. 2A, purple line). The phase-separation between Au and Ir is further corroborated by HRTEM characterization on an evolved Au-Ir catalyst particle. As shown in Figure 2B and 2C, the particle is polycrystalline with Ir and Au lattices both observable in the particle. Fast Fourier transformation (FFT) of one Au domain indicates that it is oriented along the [011] zone axis of a fcc Au crystal structure, and FFT of the neighboring Ir domain shows reflections corresponding to fcc Ir (220) planes. Experimentally, no specific lattice orientation was observed between the Au and Ir domains around the phase boundaries. We also conducted electron diffraction on the evolved catalyst particle to further unveil the catalyst structure. As shown in Figure 2D, diffraction spots that can be assigned to fcc Au and fcc Ir were identified, which reveals the polycrystalline and phase-separation nature of the evolved Au-Ir catalyst. In addition to Au and Ir, diffraction spots corresponding to IrO_2 are also identified, suggesting that the surface of Ir is oxidized after OER tests. Collectively, the electron microscopy and diffraction studies confirm that Au and Ir maintain a phase-separated state in the evolved catalysts to form an interface-rich structure. It should be

noted that such structure could be ideal for tandem catalysis that occurs across the phase boundaries.

The OER performance of the Au-Ir catalysts was studied by performing water electrolysis in 0.1 M $HClO_4$ electrolyte using a three-electrode system in an H-cell setup. Compared with the negligible activity of carbon paper supports and Au catalyst (Fig. 3A), the polarization curve of Ir catalyst shows its activity towards OER with an overpotential of ~393 mV to achieve a current density of 10 mA/cm^2. When Au is introduced into the catalyst, the evolved heterostructured Au-Ir catalyst exhibits enhanced OER catalytic activity. In particular, the overpotential of the Au-Ir catalyst at 10 mA/cm^2 is reduced by 42 mV as compared with the benchmark Ir (Fig. 3A). Notably, the onset potentials for both Au-Ir and Ir catalysts to reach 0.2 mA/cm^2 are at approximately 1.47 V. The similar onset potentials imply that the Ir sites on the Ir domains are responsible for initiating the OER process while Au has not altered the intrinsic activity of these Ir sites. When a higher potential was applied, the surface of Ir domains can be saturated with more oxygenated intermediates, which may spillover to the Au domains and subsequently desorb as O_2, thus contributing to a higher current density than pure Ir catalyst. Since the Ir mass loading on the electrodes is equal for both Au-Ir and Ir catalysts in our experiments, the OER measurements demonstrate that Au-Ir with an interface-rich structure possess a better Ir-mass-based activity (Fig. 3B and S7). At an overpotential of 300 mV, the Ir-mass-based activity of Au-Ir catalyst (0.259 A/mg$_{Ir}$) is about 1.47 times that of Ir catalyst (0.176 A/mg$_{Ir}$). Moreover, the Au-Ir and Ir catalysts exhibit a Tafel slope of 49.0 mV/dec and 55.8 mV/dec, respectively, confirming an improvement of the OER kinetics on the Au-Ir catalyst than on the Ir catalyst (Fig. 3C). With regard to the catalytic stability, the Au-Ir and Ir catalysts manifest comparable durability on carbon paper electrodes (Fig. 3D). After 5 h of reaction at a constant current density of 10 mA/cm^2, the potential shift of Au-Ir catalyst is less than 20 mV.

In order to unravel the underlying reason for the OER enhancement, we first analyzed the site-specific activity of the catalysts to investigate whether it is due to an increased number of surface Ir sites in the Au-Ir catalyst. Ir(III)/Ir(IV) redox peak was used to assess the number of accessible Ir sites on the catalyst surface.[17,18] As shown in the CV scans of Au-Ir and Ir catalysts (Fig. 3E and S8), the two catalysts exhibit comparable Ir(III)/Ir(IV) redox peaks, which correspond to 0.25 mmol$_{site}$/g$_{Ir}$ for the Au-Ir catalyst and 0.27 mmol$_{site}$/g$_{Ir}$ for the Ir catalyst. When the OER currents are normalized to the surface accessible Ir sites, the Au-Ir catalyst clearly shows

a higher specific activity than pure Ir catalyst (Fig. 3F). At an overpotential of 300 mV, the Ir-site-specific current of Au-Ir is 1.62 times that of Ir. In addition to the Ir(III)/Ir(IV) redox peak, we also analyzed the electrochemical surface area (ECSA) of the catalysts by hydrogen underpotential deposition (Fig. S9).[18,20] The measured ECSA for Au-Ir and Ir are 28.2 m^2/g_{Ir} and 30.7 m^2/g_{Ir}, respectively. With respect to the ECSA-specific activity, Au-Ir has an activity 1.61 times as high as Ir at an overpotential of 300 mV. Taken together, the analyses of surface catalytic sites based on Ir(III)/Ir(IV) redox peak and H_{upd} reveal that the number of exposed Ir sites is indeed slightly decreased in the Au-Ir catalysts. Therefore, we can rule out the number of surface-Ir sites as the factor leading to the OER enhancement.

Next, to understand whether the electronic structure of Ir sites is optimized after introducing Au into the catalysts (Fig. S10-S12), we performed X-ray photoelectron spectroscopy study on the Au-Ir catalysts and their monometallic counterparts. In the XPS spectrum of Au-Ir catalysts before OER tests, the Au $4f_{7/2}$ and Ir $4f_{7/2}$ peaks are found at 84.3 eV and 61.3 eV, respectively (Fig. S11), indicating that the Au-Ir catalysts synthesized by thermal decomposition are in a metallic state. After the catalysts were tested with OER, the Au $4f_{7/2}$ peaks in the spectra of Au-Ir and Au catalysts shift to 84.5 eV (Fig. S12A). This is possibly due to the slight surface oxidation of Au after being applied with highly positive potentials in the OER tests. The Ir 4f spectra of Au-Ir and Ir catalysts clearly evidence the oxidation of surface Ir sites in the catalysts after OER tests (Fig. S12B). Specifically, the Ir $4f_{7/2}$ peak can be deconvoluted into two peaks at 61.3 eV and 62.3 eV, which can be assigned to Ir(0) and Ir(IV),[26,42] respectively. It has been reported that the Ir(IV) oxide layer formed during the reaction is active for OER.[26,43-47] Catalysts with a higher fraction of surface Ir(IV) species possess more catalytic active sites and thus will show higher OER activity. With respect to the Ir and Au-Ir catalysts, no significant difference was observed between their XPS spectra. Both of the two catalysts contain ~90% of Ir(IV) species and ~10% of Ir(0) species after OER tests (Fig. S12 and S13). Therefore, the majority of surface Ir atoms in the Au-Ir catalysts have the same electronic structure as compared with those in the Ir catalysts. The intrinsic activity of most Ir sites in the Au-Ir catalysts has not been altered. This result is reasonable when considering that most surface Ir atoms are located on the Ir domain and do not have a direct contact with Au in the Au-Ir catalysts. Combining the XPS analysis and the electrochemical study on the site-specific activity, we conclude that the presence of Au-Ir phase boundary is the sole factor leading to the OER enhancement in the evolved Au-Ir catalysts. The

interface-enhanced OER is potentially attributable to two reasons. First, the combination of a H_2O-dissociation Ir domain with a O_2-formation Au domain allows the OER to be performed in a cooperative manner across the Au-Ir interface to enhance the overall OER kinetics (Fig. 1A). Second, for the Ir atoms at the Au-Ir phase boundaries, the intrinsic activity of these Ir sites may be improved due to the charge transfer between Au and Ir.[20,21,33] It should be noted that although the interface-rich structures were obtained via catalyst evolution on carbon paper electrodes, the limited stability of carbon may restrict its application in water electrolyzers. Since Au-Ir interface is the key structural feature, interface-rich catalysts such as Au-Ir heterodimer nanoparticles may be designed as efficient OER catalysts if non-carbon substrates are used as electrodes.

To further verify that the OER activity of Ir catalysts can be enhanced by forming phase boundaries with Au, we investigated other heterostructured catalysts that combine Au and Ir-based alloys. IrCo, IrNi, and IrCu alloy catalysts were chosen because these catalysts were reported to exhibit better OER activity than Ir,[22,23,26] owing to the optimized Ir electronic structure via the alloying with non-noble metals, and the increased the number of exposed Ir sites via the leaching of non-noble metals in acidic media. Experimentally, the multimetallic catalysts were prepared by drop-casting a mixture of metal salt precursors onto carbon papers and then thermally annealing the carbon papers under flowing Ar/H_2. The thermal treatment provides sufficient energy to the multimetallic systems, allowing them to form alloyed or phase-separated structures depending on the compatibility of the metals.[48-50] In terms of the metal compatibility, Co and Ni are highly immiscible with Au across a broad compositional and temperature range.[41] Meanwhile, both Co and Ni are miscible with Ir. Therefore, the combination of AuIrCo or AuIrNi will lead to heterostructured catalysts consisting of Au domains and IrCo alloy domains or Au domains and IrNi alloy domains, respectively. In contrast, Cu is miscible with either Au or Ir,[41] so that the combination of AuIrCu will result in heterostructured catalysts consisting of AuCu alloy domains and IrCu alloy domains. HAADF-STEM, EDS, and XRD characterizations were carried out on the multimetallic catalysts, which validated the formation of multimetallic alloyed or phase-separated catalysts as expected (Fig. 4A, 4B, and S14-S16). Specifically, IrCo, IrNi, and IrCu form alloy catalysts while Au-IrCo, Au-IrNi, and AuCu-IrCu form heterostructured catalysts (different phases are separated by the sign "-"). The OER activity of the catalysts was evaluated by conducting water electrolysis in 0.1 M $HClO_4$ solution. The loading of Ir was kept the same (~11.0 $\mu g_{Ir}/cm^2$) for all the samples to ensure a reasonable comparison. As shown in Fig. 4C and 4D, the

polarization curves of IrCo and IrNi exhibit a better OER performance than Ir. Compared with the ~393 mV overpotential of Ir at 10 mA/cm^2, the overpotentials of IrCo and IrNi are reduced to ~355 mV and ~357 mV, respectively. The OER performance of IrCu is not improved over that of Ir, which shows an overpotential increased to ~400 mV at 10 mA/cm^2. After introducing Au into the Ir-based bimetallic alloy catalysts (IrCo, IrNi, and IrCu), the heterostructured trimetallic catalysts (Au-IrCo, Au-IrNi, and AuCu-IrCu) exhibit better OER activity than corresponding bimetallic catalysts. The overpotentials of Au-IrCo, Au-IrNi, and AuCu-IrCu catalysts to obtain 10 mA/cm^2 are reduced to ~330 mV, ~335 mV, and ~376 mV, respectively (Fig. 4D). As such, the study on trimetallic catalysts corroborates that the OER activity of Ir-based alloy catalysts can be enhanced by forming heterostructures with Au, which provides a promising way to devise efficient OER catalysts in acidic conditions. Given the broad applicability of this strategy, we envision that more efficient OER catalysts may be realized if state-of-the-art Ir-based nanoparticle catalysts[23,26,28] can be combined with Au to form heterostructured nanocatalysts.

In summary, we have demonstrated that Au-Ir phase-separated catalysts with an interface-enriched structure exhibit better OER performance than Ir catalysts. Electron microscopy, X-ray spectroscopy, and electrochemical analysis were combined to reveal the central role of Au-Ir interface in achieving the enhancement of OER activity. We hypothesize that the combination of H_2O-dissociation on the Ir domain and O_2-formation on the Au domain allows the OER to be performed across the Au-Ir interface in a tandem manner, thus circumventing the scaling relation limit of Ir catalysts and boosting the overall OER kinetics. Importantly, this strategy not only works for Ir catalysts, but has also been applied to improve the OER performance of Ir-based alloy catalysts, including IrCo, IrNi, and IrCu. Taken together, our study illustrates a simple and effective way to devise OER catalysts via the cooperation of catalytic sites with different O-affinity, which, from a broader perspective, highlights the utility of tandem catalysis in overcoming the scaling relation limit of conventional electrocatalysts.

ASSOCIATED CONTENT

Supporting Information.

The Supporting Information is available free of charge on the ACS Publications website. HAADF-STEM images and EDS analysis of Au-Ir catalysts, XPS analysis of Au-Ir catalysts, ECSA analysis of Au-Ir catalysts based on H_{upd}, effect of Au-doping on the OER activity of Ir catalysts, XRD patterns of trimetallic catalysts.

AUTHOR INFORMATION

Corresponding Author

*Peidong Yang; Email: p_yang@berkeley.edu

Author Contributions

The manuscript was written through contributions of all authors. All authors have given approval to the final version of the manuscript.

Notes

The authors declare no competing financial interest.

ACKNOWLEDGMENT

This work was partially supported by the U.S. Department of Energy, Office of Science, Basic Energy Sciences, Materials Sciences and Engineering Division under Contract No. DE-AC02-05-CH11231 within the Structure and Dynamics of Materials Interfaces program KC31SM. P.-C.C. acknowledges support from Kavli ENSI Heising-Simons Fellowship. J.J. and C.C. acknowledge fellowship support from Suzhou Industrial Park. S.Y. acknowledges support from Samsung Scholarship. Work at the Molecular Foundry was supported by the Office of Science, Office of Basic Energy Sciences, of the U.S. Department of Energy under Contract No. DE-AC02-05CH11231.

REFERENCES

(1) Carmo, M.; Fritz, D. L.; Merge, J.; Stolten, D., A comprehensive review on PEM water electrolysis. *Int. J. Hydrogen Energy* **2013,** *38* (12), 4901-4934.

(2) King, L. A.; Hubert, M. A.; Capuano, C.; Manco, J.; Danilovic, N.; Valle, E.; Hellstern, T. R.; Ayers, K.; Jaramillo, T. F., A non-precious metal hydrogen catalyst in a commercial polymer electrolyte membrane electrolyser. *Nat. Nanotechnol.* **2019,** *14* (11), 1071-1074.

(3) Reier, T.; Nong, H. N.; Teschner, D.; Schlogl, R.; Strasser, P., Electrocatalytic Oxygen Evolution Reaction in Acidic Environments - Reaction Mechanisms and Catalysts. *Adv. Energy Mater.* **2017,** *7* (1), 1601275.

(4) Suen, N. T.; Hung, S. F.; Quan, Q.; Zhang, N.; Xu, Y. J.; Chen, H. M., Electrocatalysis for the oxygen evolution reaction: recent development and future perspectives. *Chem. Soc. Rev.* **2017,** *46* (2), 337-365.

(5) An, L.; Wei, C.; Lu, M.; Liu, H. W.; Chen, Y. B.; Scherer, G. G.; Fisher, A. C.; Xi, P. X.; Xu, Z. C. J.; Yan, C. H., Recent Development of Oxygen Evolution Electrocatalysts in Acidic Environment. *Adv. Mater.* **2021,** *33* (20), 2006328.

(6) Song, J. J.; Wei, C.; Huang, Z. F.; Liu, C. T.; Zeng, L.; Wang, X.; Xu, Z. C. J., A review on fundamentals for designing oxygen evolution electrocatalysts. *Chem. Soc. Rev.* **2020,** *49* (7), 2196-2214.

(7) Gu, X. K.; Camayang, J. C. A.; Samira, S.; Nikolla, E., Oxygen evolution electrocatalysis using mixed metal oxides under acidic conditions: Challenges and opportunities. *J. Catal.* **2020,** *388*, 130-140.

(8) Li, L. G.; Wang, P. T.; Shao, Q.; Huang, X. Q., Metallic nanostructures with low dimensionality for electrochemical water splitting. *Chem. Soc. Rev.* **2020,** *49* (10), 3072-3106.

(9) Dickens, C. F.; Kirk, C.; Norskov, J. K., Insights into the Electrochemical Oxygen Evolution Reaction with ab Initio Calculations and Microkinetic Modeling: Beyond the Limiting Potential Volcano. *J. Phys. Chem. C* **2019,** *123* (31), 18960-18977.

(10) Exner, K. S.; Over, H., Beyond the Rate-Determining Step in the Oxygen Evolution Reaction over a Single-Crystalline IrO2(110) Model Electrode: Kinetic Scaling Relations. *ACS Catal.* **2019,** *9* (8), 6755-6765.

(11) Rossmeisl, J.; Logadottir, A.; Norskov, J. K., Electrolysis of water on (oxidized) metal surfaces. *Chem. Phys.* **2005,** *319* (1-3), 178-184.

(12) Rossmeisl, J.; Qu, Z. W.; Zhu, H.; Kroes, G. J.; Norskov, J. K., Electrolysis of water on oxide surfaces. *J. Electroanal. Chem.* **2007,** *607* (1-2), 83-89.

(13) Man, I. C.; Su, H. Y.; Calle-Vallejo, F.; Hansen, H. A.; Martinez, J. I.; Inoglu, N. G.; Kitchin, J.; Jaramillo, T. F.; Norskov, J. K.; Rossmeisl, J., Universality in Oxygen Evolution Electrocatalysis on Oxide Surfaces. *ChemCatChem* **2011,** *3* (7), 1159-1165.

(14) Seh, Z. W.; Kibsgaard, J.; Dickens, C. F.; Chorkendorff, I. B.; Norskov, J. K.; Jaramillo, T. F., Combining theory and experiment in electrocatalysis: Insights into materials design. *Science* **2017,** *355* (6321), eaad4998.

(15) Perez-Ramirez, J.; Lopez, N., Strategies to break linear scaling relationships. *Nat. Catal.* **2019,** *2* (11), 971-976.

(16) Vojvodic, A.; Norskov, J. K., New design paradigm for heterogeneous catalysts. *Natl. Sci. Rev.* **2015,** *2* (2), 140-143.

(17) Nong, H. N.; Reier, T.; Oh, H. S.; Gliech, M.; Paciok, P.; Vu, T. H. T.; Teschner, D.; Heggen, M.; Petkov, V.; Schlogl, R.; Jones, T.; Strasser, P., A unique oxygen ligand environment facilitates water oxidation in hole-doped IrNiOx core-shell electrocatalysts. *Nature Catalysis* **2018,** *1* (11), 841-851.

(18) Nong, H. N.; Gan, L.; Willinger, E.; Teschner, D.; Strasser, P., IrOx core-shell nanocatalysts for cost- and energy-efficient electrochemical water splitting. *Chem. Sci.* **2014,** *5* (8), 2955-2963.

(19) Park, J.; Sa, Y. J.; Baik, H.; Kwon, T.; Joo, S. H.; Lee, K., Iridium-Based Multimetallic Nanoframe@Nanoframe Structure: An Efficient and Robust Electrocatalyst toward Oxygen Evolution Reaction. *ACS Nano* **2017,** *11* (6), 5500-5509.

(20) Wang, H. M.; Chen, Z. N.; Wu, D. S.; Cao, M. N.; Sun, F. F.; Zhang, H.; You, H. H.; Zhuang, W.; Cao, R., Significantly Enhanced Overall Water Splitting Performance by Partial Oxidation of Ir through Au Modification in Core-Shell Alloy Structure. *J. Am. Chem. Soc.* **2021,** *143* (12), 4639-4645.

(21) Zhao, C. X.; E, Y. F.; Fan, L. Z., Enhanced electrochemical evolution of oxygen by using nanoflowers made from a gold and iridium oxide composite. *Microchim. Acta* **2012,** *178* (1-2), 107-114.

(22) Pi, Y. C.; Shao, Q.; Wang, P. T.; Guo, J.; Huang, X. Q., General Formation of Monodisperse IrM (M = Ni, Co, Fe) Bimetallic Nanoclusters as Bifunctional Electrocatalysts for Acidic Overall Water Splitting. *Adv. Funct. Mater.* **2017,** *27* (27), 1700886.

(23) Feng, J. R.; Lv, F.; Zhang, W. Y.; Li, P. H.; Wang, K.; Yang, C.; Wang, B.; Yang, Y.; Zhou, J. H.; Lin, F.; Wang, G. C.; Guo, S. J., Iridium-Based Multimetallic Porous Hollow Nanocrystals for Efficient Overall-Water-Splitting Catalysis. *Adv. Mater.* **2017,** *29* (47), 1703798.

(24) Diaz-Morales, O.; Raaijman, S.; Kortlever, R.; Kooyman, P. J.; Wezendonk, T.; Gascon, J.; Fu, W. T.; Koper, M. T. M., Iridium-based double perovskites for efficient water oxidation in acid media. *Nat. Commun.* **2016,** *7*, 12363.

(25) Park, J.; Choi, S.; Oh, A.; Jin, H.; Joo, J.; Baik, H.; Lee, K., Hemi-core@frame AuCu@IrNi nanocrystals as active and durable bifunctional catalysts for the water splitting reaction in acidic media. *Nanoscale Horiz.* **2019,** *4* (3), 727-734.

(26) Liu, D.; Lv, Q. Q.; Lu, S. Q.; Fang, J. J.; Zhang, Y. F.; Wang, X. D.; Xue, Y. R.; Zhu, W.; Zhuang, Z. B., IrCuNi Deeply Concave Nanocubes as Highly Active Oxygen Evolution Reaction Electrocatalyst in Acid Electrolyte. *Nano Lett.* **2021,** *21* (7), 2809-2816.

(27) Seitz, L. C.; Dickens, C. F.; Nishio, K.; Hikita, Y.; Montoya, J.; Doyle, A.; Kirk, C.; Vojvodic, A.; Hwang, H. Y.; Norskov, J. K.; Jaramillo, T. F., A highly active and stable IrOx/SrIrO3 catalyst for the oxygen evolution reaction. *Science* **2016,** *353* (6303), 1011-1014.

(28) Pi, Y. C.; Zhang, N.; Guo, S. J.; Guo, J.; Huang, X. Q., Ultrathin Laminar Ir Superstructure as Highly Efficient Oxygen Evolution Electrocatalyst in Broad pH Range. *Nano Lett.* **2016,** *16* (7), 4424-4430.

(29) Wang, Q. L.; Xu, C. Q.; Liu, W.; Hung, S. F.; Yang, H. B.; Gao, J. J.; Cai, W. Z.; Chen, H. M.; Li, J.; Liu, B., Coordination engineering of iridium nanocluster bifunctional electrocatalyst for highly efficient and pH-universal overall water splitting. *Nat. Commun.* **2020,** *11* (1), 4246.

(30) Fu, L. H.; Zeng, X.; Cheng, G. Z.; Luo, W., IrCo Nanodendrite as an Efficient Bifunctional Electrocatalyst for Overall Water Splitting under Acidic Conditions. *ACS Appl. Mater. Interfaces* **2018,** *10* (30), 24993-24998.

(31) de Freitas, I. C.; Parreira, L. S.; Barbosa, E. C. M.; Novaes, B. A.; Mou, T.; Alves, T. V.; Quiroz, J.; Wang, Y. C.; Slater, T. J.; Thomas, A.; Wang, B.; Haigh, S. J.; Camargo, P. H. C., Design-controlled synthesis of IrO2 sub-monolayers on Au nanoflowers: marrying plasmonic and electrocatalytic properties. *Nanoscale* **2020,** *12* (23), 12281-12291.

(32) Fan, Z. X.; Luo, Z. M.; Chen, Y.; Wang, J.; Li, B.; Zong, Y.; Zhang, H., Synthesis of 4H/fcc-Au@M (M = Ir, Os, IrOs) Core-Shell Nanoribbons For Electrocatalytic Oxygen Evolution Reaction. *Small* **2016,** *12* (29), 3908-3913.

(33) Moon, S.; Cho, Y. B.; Yu, A.; Kim, M. H.; Lee, C.; Lee, Y., Single-Step Electrospun Ir/IrO2 Nanofibrous Structures Decorated with Au Nanoparticles for Highly Catalytic Oxygen Evolution Reaction. *ACS Appl. Mater. Interfaces* **2019,** *11* (2), 1979-1987.

(34) Kim, S.; Cho, M.; Lee, Y., Iridium Oxide Dendrite as a Highly Efficient Dual Electro-Catalyst for Water Splitting and Sensing of H2O2. *J. Electrochem. Soc.* **2017,** *164* (5), B3029-B3035.

(35) Zhang, X. B.; Han, S. B.; Zhu, B. E.; Zhang, G. H.; Li, X. Y.; Gao, Y.; Wu, Z. X.; Yang, B.; Liu, Y. F.; Baaziz, W.; Ersen, O.; Gu, M.; Miller, J. T.; Liu, W., Reversible loss of core-shell structure for Ni-Au bimetallic nanoparticles during CO2 hydrogenation. *Nat. Catal.* **2020,** *3* (4), 411-417.

(36) Wang, P. K.; Chang, F.; Gao, W. B.; Guo, J. P.; Wu, G. T.; He, T.; Chen, P., Breaking scaling relations to achieve low-temperature ammonia synthesis through LiH-mediated nitrogen transfer and hydrogenation. *Nat. Chem.* **2017,** *9* (1), 64-70.

(37) Yamada, Y.; Tsung, C. K.; Huang, W.; Huo, Z. Y.; Habas, S. E.; Soejima, T.; Aliaga, C. E.; Somorjai, G. A.; Yang, P. D., Nanocrystal bilayer for tandem catalysis. *Nat. Chem.* **2011,** *3* (5), 372-376.

(38) Xie, C. L.; Chen, C.; Yu, Y.; Su, J.; Li, Y. F.; Somorjai, G. A.; Yang, P. D., Tandem Catalysis for CO_2 Hydrogenation to C2-C4 Hydrocarbons. *Nano Lett.* **2017,** *17* (6), 3798-3802.

(39) Subbaraman, R.; Tripkovic, D.; Strmcnik, D.; Chang, K. C.; Uchimura, M.; Paulikas, A. P.; Stamenkovic, V.; Markovic, N. M., Enhancing Hydrogen Evolution Activity in Water Splitting by Tailoring Li+-Ni(OH)(2)-Pt Interfaces. *Science* **2011,** *334* (6060), 1256-1260.

(40) Chen, C. B.; Li, Y. F.; Yu, S.; Louisia, S.; Jin, J. B.; Li, M. F.; Ross, M. B.; Yang, P. D., Cu-Ag Tandem Catalysts for High-Rate CO_2 Electrolysis toward Multicarbons. *Joule* **2020,** *4* (8), 1688-1699.

(41) Okamoto, H.; Schlesinger, M. E.; Mueller, E. M. Eds. *Alloy Phase Diagrams*; ASM Handbook Vol.3; ASM International: Materials Park, OH, U.S.A., 2016.

(42) Zhao, Y.; Luo, M.; Chu, S. F.; Peng, M.; Liu, B. Y.; Wu, Q. L.; Liu, P.; de Groot, F. M. F.; Tan, Y. W., 3D nanoporous iridium-based alloy microwires for efficient oxygen evolution in acidic media. *Nano Energy* **2019,** *59*, 146-153.

(43) Pavlovic, Z.; Ranjan, C.; van Gastel, M.; Schlogl, R., The active site for the water oxidising anodic iridium oxide probed through in situ Raman spectroscopy. *Chem. Commun.* **2017,** *53* (92), 12414-12417.

(44) Lettenmeier, P.; Majchel, J.; Wang, L.; Saveleva, V. A.; Zafeiratos, S.; Savinova, E. R.; Gallet, J. J.; Bournel, F.; Gago, A. S.; Friedrich, K. A., Highly active nano-sized iridium catalysts: synthesis and operando spectroscopy in a proton exchange membrane electrolyzer. *Chem. Sci.* **2018,** *9* (14), 3570-3579.

(45) Naito, T.; Shinagawa, T.; Nishimoto, T.; Takanabe, K., Recent advances in understanding oxygen evolution reaction mechanisms over iridium oxide. *Inorg. Chem. Front.* **2021,** *8* (11), 2900-2917.

(46) Oh, H. S.; Nong, H. N.; Reier, T.; Bergmann, A.; Gliech, M.; de Araujo, J. F.; Willinger, E.; Schlogl, R.; Teschner, D.; Strasser, P., Electrochemical Catalyst-Support Effects and Their Stabilizing Role for IrOx Nanoparticle Catalysts during the Oxygen Evolution Reaction. *J. Am. Chem. Soc.* **2016,** *138* (38), 12552-12563.

(47) Kasian, O.; Grote, J. P.; Geiger, S.; Cherevko, S.; Mayrhofer, K. J. J., The Common Intermediates of Oxygen Evolution and Dissolution Reactions during Water Electrolysis on Iridium. *Angew. Chem. Int. Ed.* **2018,** *57* (9), 2488-2491.

(48) Chen, P. C.; Liu, X. L.; Hedrick, J. L.; Xie, Z.; Wang, S. Z.; Lin, Q. Y.; Hersam, M. C.; Dravid, V. P.; Mirkin, C. A., Polyelemental nanoparticle libraries. *Science* **2016,** *352* (6293), 1565-1569.

(49) Chen, P. C.; Liu, M. H.; Du, J. S. S.; Meckes, B.; Wang, S. Z.; Lin, H. X.; Dravid, V. P.; Wolverton, C.; Mirkin, C. A., Interface and heterostructure design in polyelemental nanoparticles. *Science* **2019,** *363* (6430), 959-964.

(50) Du, J. S.; Chen, P. C.; Meckes, B.; Xie, Z.; Zhu, J. H.; Liu, Y.; Dravid, V. P.; Mirkin, C. A., The Structural Fate of Individual Multicomponent Metal-Oxide Nanoparticles in Polymer Nanoreactors. *Angew. Chem. Int. Ed.* **2017,** *56* (26), 7625-7629.

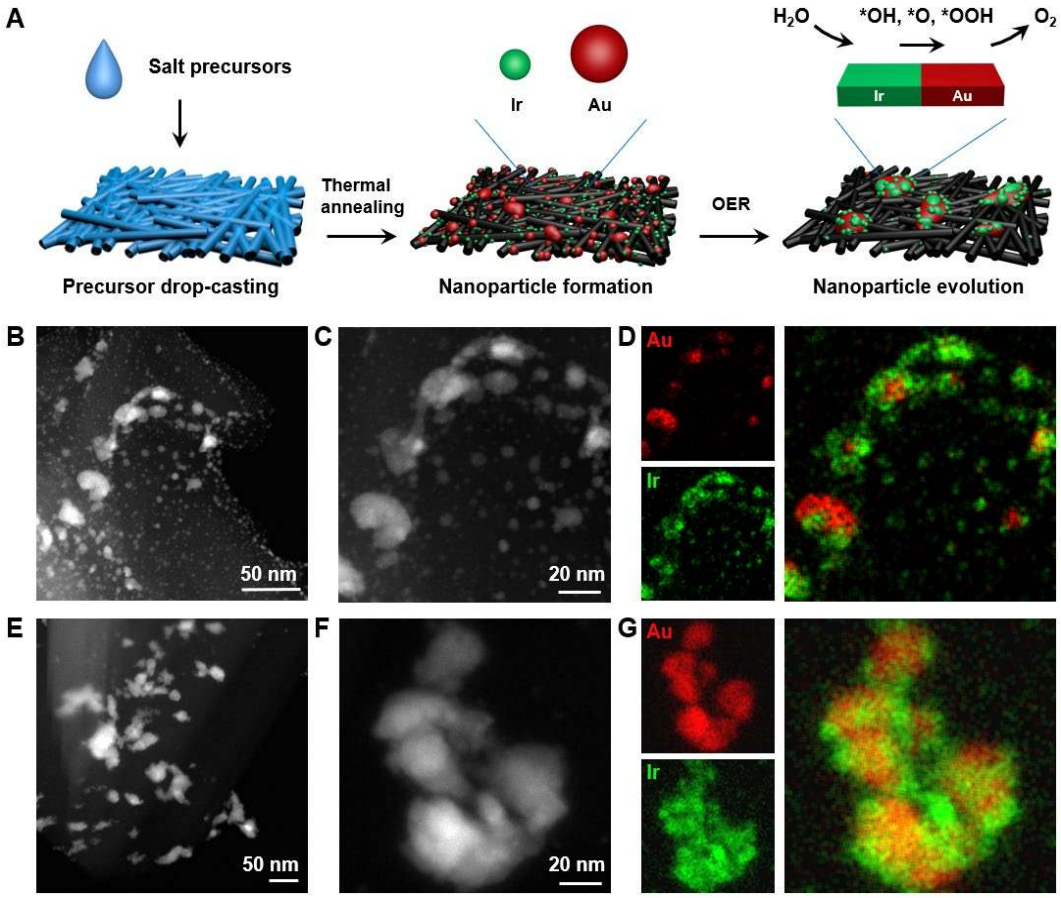

Figure 1. Au-Ir catalyst synthesis and evolution. (A) Scheme depicting the preparation of Au and Ir catalysts on carbon paper supports and their structural transformation into heterostructured Au-Ir particles in OER measurements. (B,C) Low- and high-magnification HAADF-STEM images of as-synthesized Au-Ir catalysts. (D) EDS elemental mapping of the catalysts shown in (C). (E,F) Low- and high-magnification HAADF-STEM images of Au-Ir catalysts after OER tests. (G) EDS elemental mapping of the catalysts shown in (F).

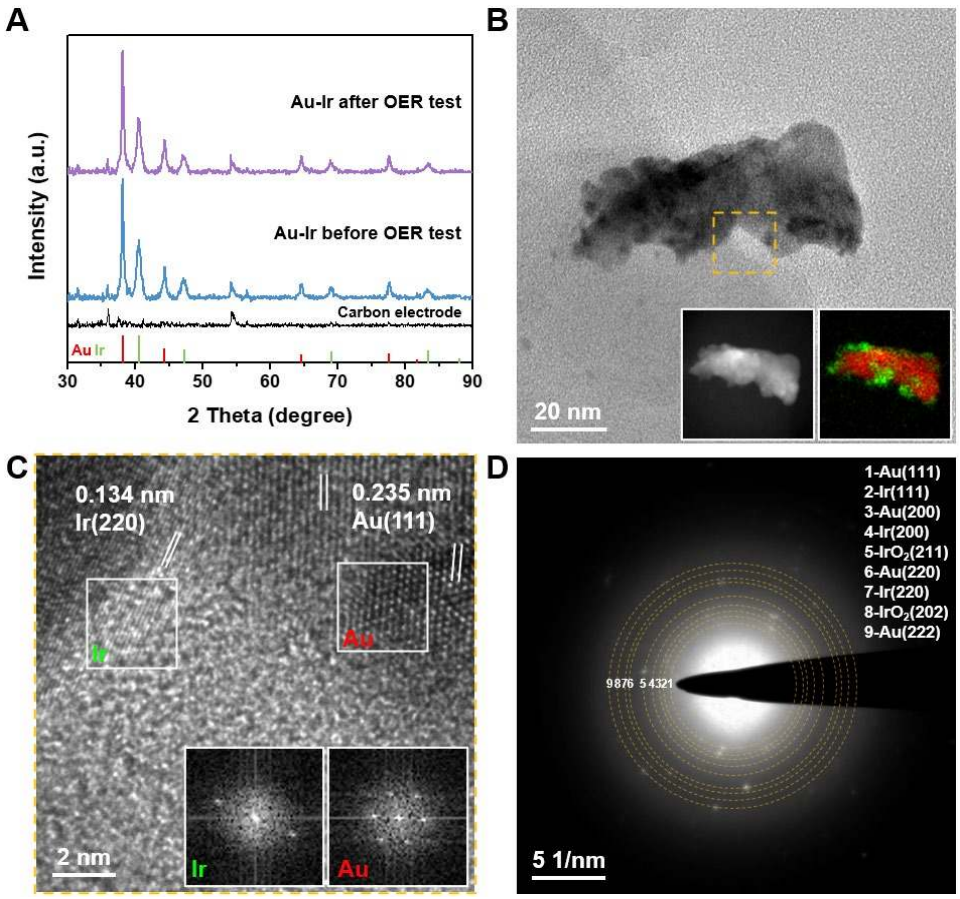

Figure 2. Structural characterization of heterostructured Au-Ir catalysts. (A) XRD patterns of carbon paper supports, and Au-Ir catalysts before and after OER tests. (B) TEM image of a representative Au-Ir heterostructured particle formed after OER test. Insets are HAADF-STEM image and EDS mapping of the particle. (C) HRTEM image of the region indicated by a yellow dashed square in the particle shown in (B). Insets are FFT of the regions indicated by white squares in the HRTEM image. (D) Electron diffraction pattern of the particle shown in (B).

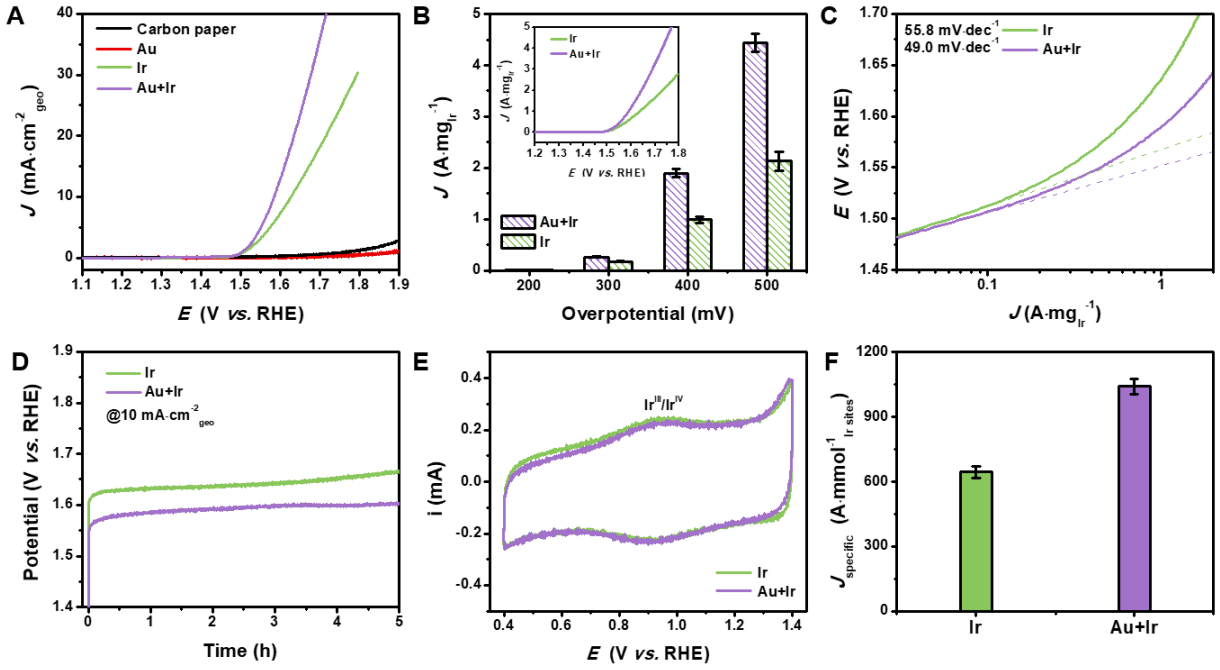

Figure 3. OER performance of heterostructured Au-Ir catalysts. (A) OER polarization curves of different catalysts in 0.1 M $HClO_4$ solution. Scan rate: 5 mV/s. (B) Ir-mass-based OER activities of Ir and Au-Ir catalysts. (C) Corresponding Tafel plots of Ir and Au-Ir catalysts. (D) Chronopotentiometric measurements of Ir and Au-Ir catalysts at a current density of 10 mA/cm^2. (E) CV curves of Ir and Au-Ir catalysts in 0.1 M $HClO_4$ solution showing the Ir(III)/Ir(IV) redox peak. (F) Specific OER activities of Ir and Au-Ir catalysts at an overpotential of 300 mV that are normalized to the surface accessible Ir sites.

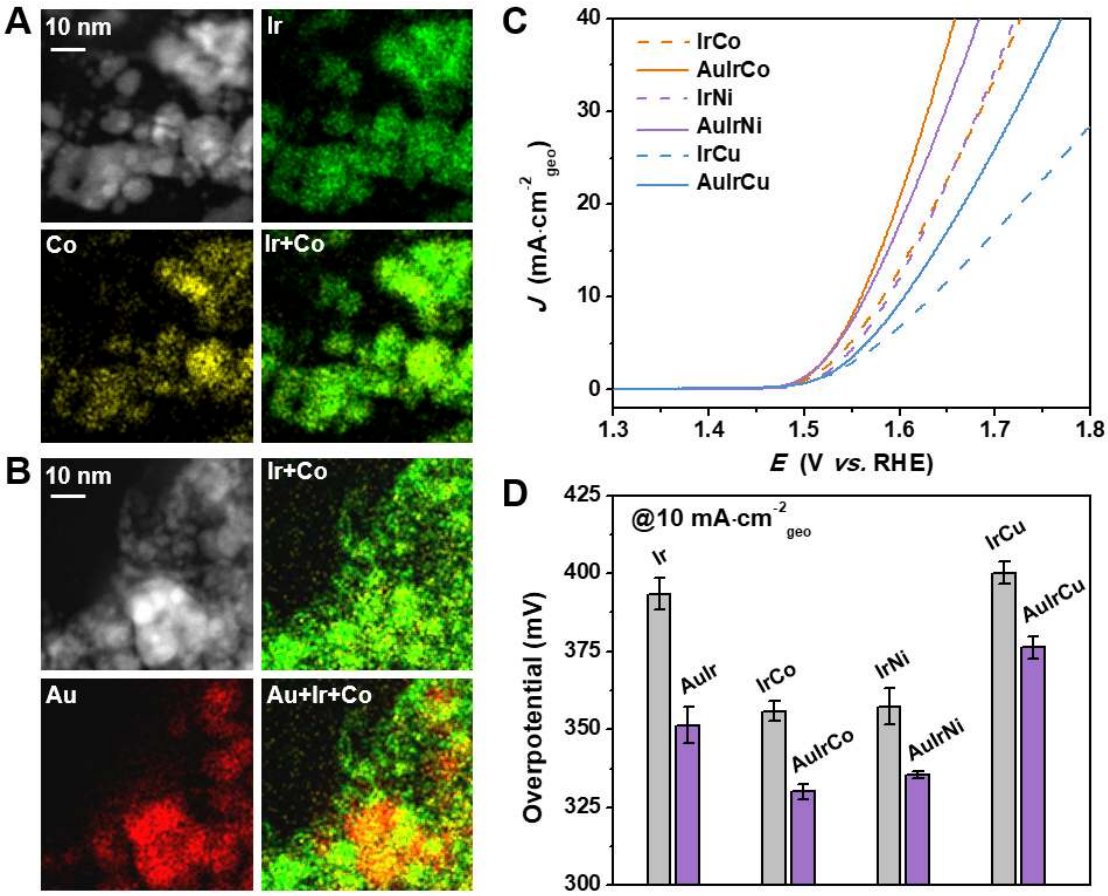

Figure 4. Ir-based multimetallic catalysts for enhanced OER. (A,B) HAADF-STEM images and EDS elemental mapping of (A) IrCo and (B) AuIrCo catalysts after OER tests. (C) OER polarization curves of Ir-based catalysts in 0.1 M $HClO_4$ solution. Scan rate: 5 mV/s. (D) Overpotentials of different Ir-based catalysts at a current density of 10 mA/cm^2.

Table of Contents Graphic